ELSEVIER

Polymer 41 (2000) 8953–8960

polymer

www.elsevier.nl/locate/polymer

Phase transformations in a chiral main-chain liquid crystalline polyester involving double-twist helical crystals ☆

C.Y. Li[a], J.J. Ge[a], F. Bai[a], J.Z. Zhang[a], B.H. Calhoun[a], L.-C. Chien[b], F.W. Harris[a], B. Lotz[c], S.Z.D. Cheng[a,*]

[a]*The Maurice Morton Institute and Department of Polymer Science, The University of Akron, Akron, OH 44325-3909, USA*
[b]*Liquid Crystal Institute, Kent State University, Kent, OH 44010-0001, USA*
[c]*Institute Charles Sadron, 6 Rue Boussingault, Strasbourg 67083, France*

Received 4 October 1999; received in revised form 11 February 2000; accepted 15 February 2000

Abstract

A main-chain non-racemic chiral liquid crystalline polymer has been synthesized from (*R*)-(−)-4′-{ω-[2-(p-hydroxy-*o*-nitrophenyloxy)-1-propyloxy]-1-nonyloxy}-4-biphenyl carboxylic acid, abbreviated PET(R*)-9. Based on differential scanning calorimetry, wide angle X-ray diffraction (WAXD) and polarized light microscopy experiments, this polymer undergoes at least three liquid crystalline (LC) transitions in addition to crystallization. The LC transition sequence is

$$\mathrm{I} \underset{3.21\ \mathrm{kJ/mol}}{\overset{185^{\circ}\mathrm{C}}{\leftrightarrow}} \mathrm{TGBA}^{*} \underset{1.27\ \mathrm{kJ/mol}}{\overset{175^{\circ}\mathrm{C}}{\leftrightarrow}} \mathrm{S}_{\mathrm{A}}^{*} \underset{0.35\ \mathrm{kJ/mol}}{\overset{130^{\circ}\mathrm{C}}{\leftrightarrow}} \mathrm{S}_{\mathrm{C}}^{*} \overset{37^{\circ}\mathrm{C}}{\leftrightarrow} T_{\mathrm{g}}$$

The transition sequence is reversible since they are LC phases, which are close to thermodynamic equilibrium. Among these phases, the twisted grain boundary smectic A (TGBA*) phase is, for the first time, found in a main-chain LC polymer. The TGBA* is only stable within a temperature region of 10°C between the Smectic A* (S_A^*) phase and the isotropic melt. Crystallization that takes place in the (S_A^*) phase can form both flat-elongated and double-twist helical single lamellar crystals, as observed by transmission electron microscopy (TEM). Analysis of the WAXD fiber patterns of this polymer indicates that the crystal structure of PET(R*)-9 in the bulk is orthorhombic, identical with that determined using selective area electron diffraction in TEM [Macromolecules 32 (1999) 524; Phys Rev B 60 (1999) 12 675]. © 2000 Elsevier Science Ltd. All rights reserved.

Keywords: Phase transformations; Liquid crystalline polyester; Double-twist helical crystals

1. Introduction

Over the past two years, we have focused on the study of one non-racemic chiral main-chain liquid crystalline (LC) polyester synthesized from (R)-(−)-4′-{ω-[2-(*p*-hydroxy-*o*-nitrophenyloxy)-1-propyloxy]-1-nonyloxy}-4-biphenyl carboxylic acid, abbreviated PET(R*)-9 [1–5]. The polymer repeat unit chemical structure is:

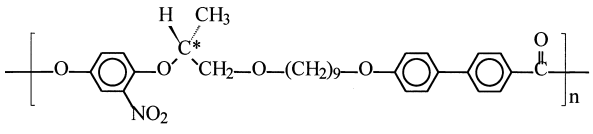

For the first time, both flat-elongated and helical single lamellar crystals have been thermotropically grown under the same crystallization condition as shown in Fig. 1 [1,2]. Surprisingly, these crystals possess the same structure, which is an orthorhombic lattice with the three dimensional sizes of the crystal unit cell $a = 1.07$, $b = 0.48$ and $c = 5.96$ nm [1,2]. The polymer chain folding direction in both flat and helical lamellar crystals is also determined to be identical, and it is always along the long axis of the lamellar crystals [1,2].

Recent dark field (DF) image, bright field image, and selective area electron diffraction (SAED) experiments in transmission electron microscopy (TEM) provide chain orientation information for both the flat-elongated and helical lamellar crystals [3,4]. In the flat-elongated lamellar crystals, the chain direction is only perpendicular to the substrate surface in a near center zone along the long axis of the crystals [4]. Moving away from this zone along the

☆ In memory of Professor Andrew Keller for his great lifetime contributions to polymer physics and many years of friendship and collaborations.

* Corresponding author. Tel.: +1-330-972-6931; fax: +1-330-972-8626.
E-mail address: cheng@polymer.uakron.edu (S.Z.D. Cheng).

PII: S0032-3861(00)00238-X

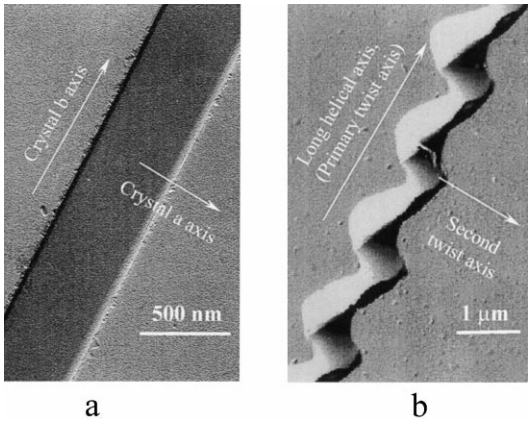

Fig. 1. Flat-elongated and helical lamellar morphologies observed under TEM. The thin film sample was crystallized at 145°C for one day.

short axis of the crystal, the chain direction continuously tilts in the *ac*-plane. A small tilt angle of approximately 0.002° per molecular layer can be estimated using the SAED results [4]. In the helical lamellar crystals, the main twist direction is parallel to the long helical axis, and the rotating angle for each molecular layer is approximately 0.05° [3,4]. However, specifically designed DF experiments using the entire and partial (205) and (206) diffraction arcs show that the chain orientation direction is also twisted along the short helical axis of the lamellar crystal. The rotating angle is approximately 0.01° per molecular layer. This leads to a second twist direction in addition to the twist along the long helical axis of the crystal [3,4]. Based on these experimental observations, the concept of double-twist molecular orientation in the helical lamellar crystal can be established, although in principle, the macroscopic translation symmetry is broken along both the long and short axes of the helical lamellar crystals. This crystal can therefore be recognized as symmetrically "soft", rather than a true crystal based on the traditional crystal definition in Euclidean space. Mathematically, double-twist crystals can only be true crystals in Riemannian space [3,4]. Note that the double-twist was first proposed in description of condensed states in small molecular liquid crystals and biopolymers [6,7].

Upon careful examination of the crystallization behavior of PET(R*)-9, it is not difficult to find that the crystallization takes place in a LC phase instead of the isotropic melt. The crystallization behavior and crystal morphology formed may critically depend upon the molecular orientation and structural order in this LC phase. Therefore, a clear understanding of the phase structures and transformations of this polymer is necessary in order to make connections with crystal morphology. In this publication, investigations on this topic of PET(R*)-9 are reported. At least three LC phases can be identified in this polymer based on differential scanning calorimety (DSC) experiments. Their structures are characterized using techniques of wide angle X-ray diffraction (WAXD) and SAED in TEM. Morphological investigations in PLM also aid in phase identification of the LC phases.

2. Experiential section

2.1. Materials and sample preparation

The polymer reported here is synthesized from (*R*)-(−)-4′-{ω-[2-(*p*-hydroxy-*o*-nitrophenyloxy)-1-propyloxy]-1-nonyloxy}-4-biphenyl carboxylic acid. The detailed synthesis routes of the monomers and polymers are published elsewhere [1–5]. The number of methylene units in the polymer of this study is nine, and this polymer possesses right-hand chiral centers (R*) along the main-chain backbone. The specific rotation of the monomers is $[\alpha]_D = -28.5°$. Due to the head-to-tail connection of the monomers in this polymer (an A–B monomer polymerization) [1–5], the optical activity of this monomer is retained, and thus, the polymer is non-racemic chiral. The molecular weight of PET(R*)-9 is around 16,000 g/mol and the polydispersity is approximately 2 after fractionations, as measured by gel permeation chromatography based on polystyrene standards.

Polymer thin films (with a thickness of around 50–100 nm) were prepared *via* solution casting from a 0.05% (w/v) tetrahydrofuran solution. After the solvent was evaporated, the films were heated in a heating stage (Mettler FP-90) above its highest endothermic transition temperature (185°C) and were subsequently quenched to preset temperatures. The samples were held isothermally for various periods of time ranging from several minutes to a few days. Samples were then quenched in liquid nitrogen and allowed to return to room temperature, which is below the glass transition temperature of this polymer ($T_g = 37°C$). The thin film samples prepared for TEM observations were first examined under both polarized light microscopy (PLM) and phase contrast microscopy before they were shadowed by Pt and coated with carbon. For DSC and WAXD measurements, a typical bulk sample size was 2–3 mg. The samples were first heated to above the highest transition temperature to erase the thermal history. For PLM film samples, a typical thickness of 10 μm was used by melt-pressing small amounts of samples between two glass slides. Fibers were drawn from the LC phase in order to determine phase structures. A typical fiber diameter was 30 μm. Thermal histories of these samples were kept the same in these experiments.

2.2. Equipment and experiments

The thermal transition behaviors were detected using a Perkin–Elmer DSC-7. The temperature and heat flow scales at different cooling and heating rates (0.5–40°C/min) were carefully calibrated using standard materials. Cooling experiments always preceded heating experiments, and the cooling and heating rates were always kept identical. The transition temperatures were determined by measuring onset

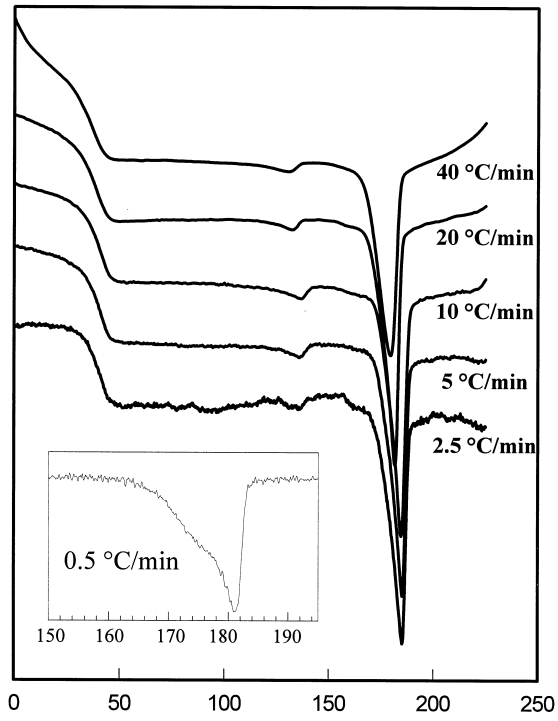

Fig. 2. A set of DSC cooling thermal diagrams for PET(R*)-9 at different rates between 2.5 and 40°C/min. The insert is a cooling diagram at a rate of 0.5°C/min.

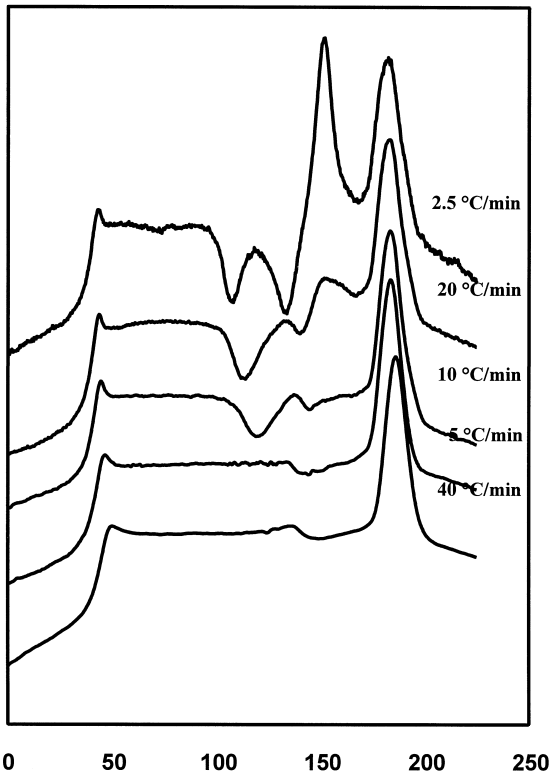

Fig. 3. A set of DSC heating thermal diagrams for PET(R*)-9 at different rates between 2.5 and 40°C/min.

and peak temperatures from cooling and heating scans at different rates. Equilibrium transition temperatures were obtained by extrapolations to 0°C/min.

Powder samples of WAXD experiments were performed with a Rigaku 12 kW rotating anode generator (CuK_α radiation) equipped with a diffractometer. A hot stage was coupled with the diffractometer to study the structural evolution with temperature at constant heating and cooling rates. The temperature was controlled to within ±1°C. Films having a thickness of approximately 0.1 mm were mounted on aluminum sheets and the diffraction patterns were collected by reflection mode. Samples were scanned in a 2θ range between 1.5 and 30°. Background scattering was subtracted from the sample diffraction patterns.

WAXD fiber patterns were obtained from a Rigaku Automated X-ray Imaging System (3000 × 3000 pixel resolution) with an 18 kW rotating anode X-ray generator. A hot stage was also coupled with the diffractometer to study the structural evolution with temperature at different temperatures. The temperature was controlled to ±1°C. A 30-min exposure was required for a high quality WAXD fiber pattern. The background scattering was again subtracted from the fiber patterns.

Phase morphology and LC textures were examined via a PLM (Olympus BH-2) and a Mettler hot stage (FP-90). TEM experiments were carried out in a JEOL (1200 EX II) TEM using an accelerating voltage of 120 kV. Calibration of the ED spacing was done using TlCl in a *d*-spacing range smaller than 0.384 nm, which is the largest spacing for TlCl. Spacing values larger than 0.384 nm were calibrated by doubling the *d*-spacing of those reflections based on their first order reflections.

3. Results and discussion

3.1. Thermodynamic transition behaviors

Figs. 2 and 3 show a set of cooling and subsequent heating DSC thermal diagrams for PET(R*)-9 at different rates between 2.5 and 40°C/min. A glass transition temperature (T_g) at 37°C is evident. When the cooling and heating rates are equal or faster than 10°C/min, there is apparently a first-order transition appearing at an onset transition temperature of 185°C during cooling and 175°C during heating. Of interest is that the onset transition temperature during cooling is higher than during heating. This is a possible indication of two overlapped first-order transitions or a bi-phasic phenomenon. If one uses a slower cooling rate of 0.5°C/min, two separated first-order transitions start to be observed (the in-set in Fig. 2). In fact, this type of observation has also been found in other LC polymers, as recently reported [6]. The enthalpy changes of these two first-order transitions are 3.21 kJ/mol (for the higher temperature transition) and 1.27 kJ/mol (for the lower temperature transition), respectively. Another transition can be found at 130°C with a small transition enthalpy change (0.35 kJ/mol). It is important to

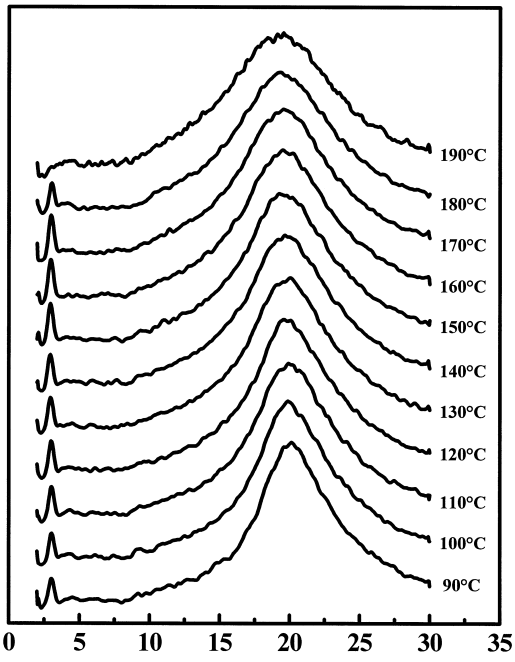

Fig. 4. Set of WAXD powder patterns for a fast cooled PET(R*)-9 sample at 20°C/min.

note that all three transitions are almost cooling and heating rate independent in the range of rates investigated, indicating that these transitions are associated with LC phase transformations, which are close to thermodynamic equilibrium.

When the DSC controlled heating rates are slower than 10°C/min, other thermal events take place (see Fig. 3). These transitions must be attributed to crystallization and melting of the crystals in this polymer since their transition temperatures and enthalpy changes are very much cooling and heating rate dependent. This is indicative of kinetically controlled transition processes. When the heating rate is 2.5°C/min, for example, an exothermic process can be found at 105°C, followed by another exothermic process at around 130°C. Both of them may represent crystallization. An endothermic process can be seen at around 160°C, possibly due to crystal melting. The samples then enter the LC phase upon further heating before the isotropic melt is reached. However, DSC thermal diagrams do not provide structural information regarding the phases and phase transformations, therefore, phase identification must rely on structural characterization techniques such as WAXD.

3.2. Identification of LC phases

Fig. 4 shows a set of WAXD powder patterns during a fast cooling from the isotropic melt to room temperature at a rate of 20°C/min. Clearly, LC phases cannot be bypassed at this cooling rate due to the near thermodynamic equilibrium nature. The WAXD powder pattern at 190°C shows evidence of a transition characterized by two features. The first feature is the appearance of a low-angle reflection at $2\theta = 3.0°$, which corresponds to a *d*-spacing of 2.96 nm. The second feature is a sudden shift of the wide-angle halo at around $2\theta = 20°$. Both features indicate a transition from the isotropic melt to a low ordered smectic LC phase, similar to other examples identified in previous publications [8–12]. When the temperature is continuously decreased to 130°C, the low-angle reflection exhibits a shift to a slightly higher angle of $2\theta = 3.05°$ (corresponding to a *d*-spacing of 2.90 nm). Furthermore, the wide-angle scattering halo becomes increasingly sharper on cooling to 130°C. Note that this transition can also be found in the DSC cooling and heating thermal diagrams (Figs. 2, 3). Detailed dimensionality of the structure of this LC phase have to be determined in the WAXD fiber pattern (see below).

Fig. 5 shows two WAXD fiber patterns obtained at different temperatures. At 160°C, the fiber pattern in Fig. 4a clearly indicates a typical smectic A (S_A) phase since the layer reflection from the low-angle is on the equator and the scattering halo is on the meridian (the reverse of these two directions will be discussed in the following section). After annealing at 120°C, however, the WAXD fiber pattern in Fig. 4b shows that the scattering halo is still on the

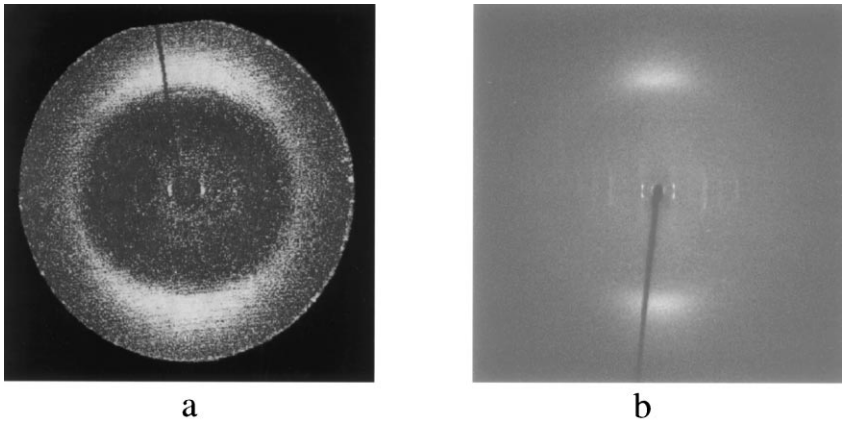

Fig. 5. Two WAXD fiber patterns for PET(R*)-9 in both of the S_A^* phase obtained at 160°C (a) and the S_C^* phase obtained at 120°C (b).

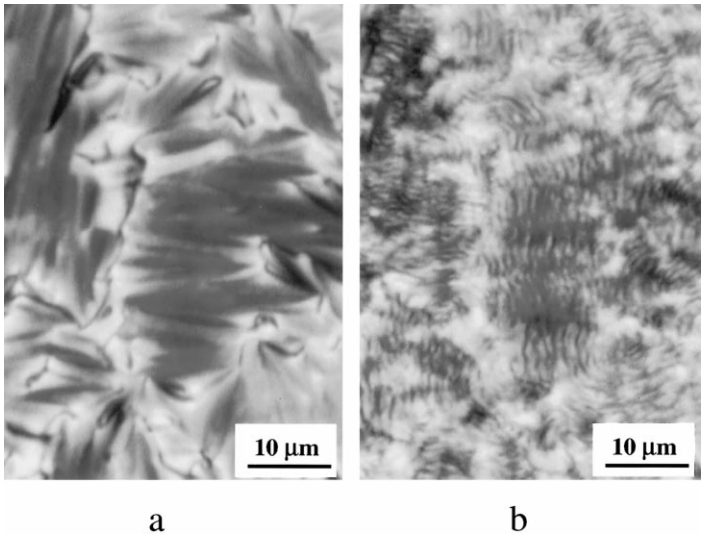

Fig. 6. PLM observations of the focal conic texture obtained at 160°C for the S_A^* phase (a) and the broken focal conic texture obtained at 120°C for the S_C^* phase (b).

meridian while the layer reflection is slightly shifted to the quadrant, which is a typical S_C pattern. The angle between the layer reflection and the meridian (the fiber direction) is 79°, indicating that the layer normal is tilted 11° away from the equator. Therefore, the transition at 130°C is a $S_A^* \leftrightarrow S_C^*$ transition. The assignments of S_A^* and S_C^* are also supported by texture observations under PLM at different temperatures. The sample was sheared and relaxed at 180°C and then slowly (1°C/min) cooled and annealed at 160 and 120°C. Fig. 6a shows a S_A^* focal conic texture formed after the sheared sample was annealed at 160°C, while this texture is broken when cooled down passing 130°C at which the phase transition takes place (Fig. 6b). The broken focal conics are indicative of the S_C^* phase which is consistent with X-ray fiber pattern results. The formation of this texture is due to the shrinkage of layer thickness during the transition.

The remaining issue is the overlapped transition that occurs between 175 and 185°C which should be associated with three phases. The highest temperature phase is the isotropic melt, while below 175°C the S_A^* exists. However, we have not identified the phase structure between 175 and 185°C. Based on WAXD results, one can conclude that this undetermined phase must also be related to the S_A^* phase since the low angle reflection at $2\theta = 3.0°$, which represents the layer structure, starts to appear at 185°C, and in fiber heating experiments, the layer reflection does not disappear until 185°C. However, since neither the WAXD powder nor the fiber patterns are sensitive to the structure changes of this transition, one speculation is that this transition must be related to the larger length scale of supra-molecular assembly rather than structures on the molecular level. The observations obtained by PLM show helical textures with alternating strong and weak birefringence as shown in Fig. 7. This LC morphology is virtually identical to the twisted grain boundary (TGB) phase morphology observed in small molecule LC and side-chain LC polymers [13,14]. Combining both observations of the PLM helical texture and the WAXD results of which the layer structure of the S_A^* phase exists between 175°C and 185°C, it is strongly suggested that the high temperature phase mediate isotropic melt and the S_A^* phase is a TGBA* phase. The issue of handedness of the texture is currently under investigation.

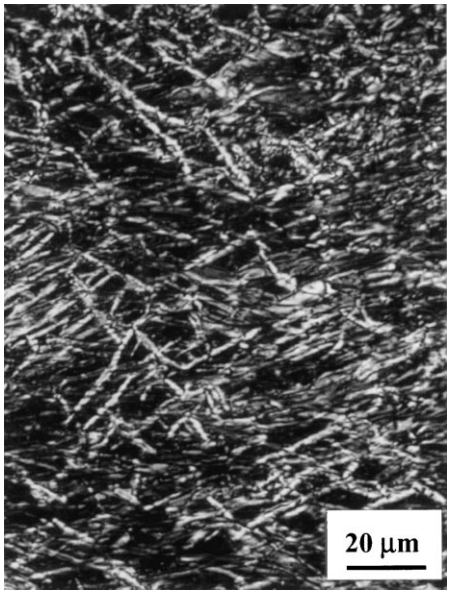

Fig. 7. Helical liquid crystalline morphology observed in PLM at 184°C.

3.3. Identification of crystalline phases

In principle, crystallization occurs between the T_g and T_m, and therefore, for this polymer, the crystallization window

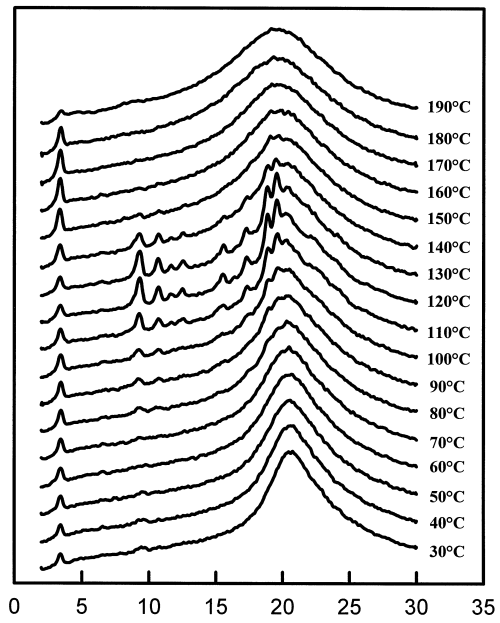

Fig. 8. Set of WAXD powder patterns during heating at 1°C/min for a quenched PET(R*)-9 sample.

should be between 37 and 170°C. However, the S_A^* phase is in the temperature region of 130 to 175°C, while the temperature region between 37 and 130°C is the S_C^* phase. As shown in Figs. 2 and 3, when the heating rate is slow (≤5°C/min), crystallization takes place. Fig. 8 shows a set of WAXD powder patterns recorded during heating at 1°C/min for a quenched PET(R*)-9 sample. When the temperature reaches 80°C, multiple reflections start to appear in the wide-angle region, indicating that crystallization is initiated. These reflections remain until the temperature approaches 170°C, at which the crystal melts. The focus here is only on the crystal structure developed from the S_A^* phase.

The crystal structure can be determined using both the

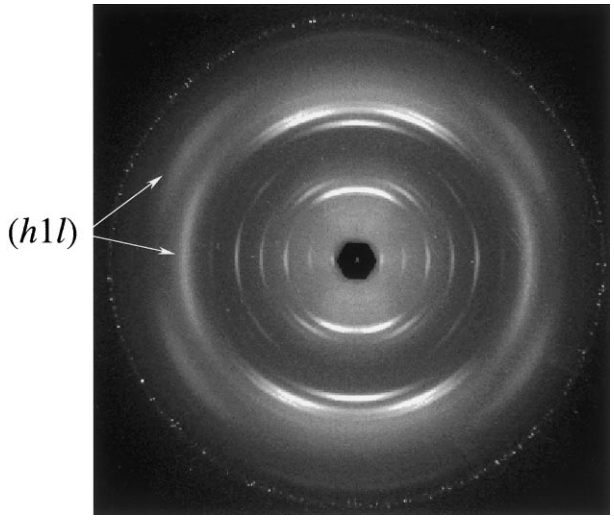

Fig. 9. A WAXD fiber pattern for a drawn PET(R*)-9 sample after it has been annealed at 145°C for one day.

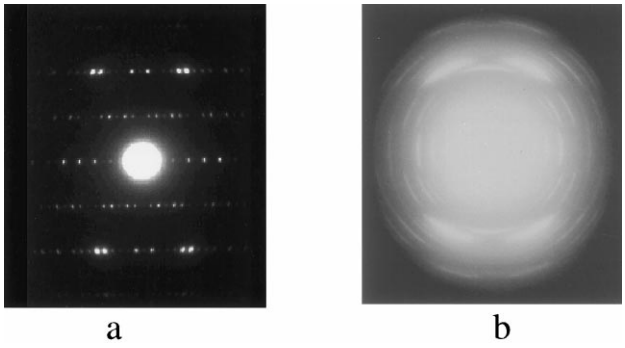

Fig. 10. SAED patterns of sheared sample with high orientation (a) and relatively low orientation (b).

SAED and WAXD techniques. Fig. 9 shows a WAXD fiber pattern that has been annealed at 145°C for one day and then quenched to room temperature. It is evident that multiple reflections can be seen. First, along the equator, reflections up to the sixth order appear, corresponding to the (00*l*) planes. Therefore, the *c*-axis dimension can be determined to be 5.96 nm, in excellent agreement with the results derived from SAED experiments [1,2]. This indicates that the fiber direction is perpendicular to the chain direction, similar to many biopolymer fibers [15]. However, it must be emphasized that in biopolymers, this kind of molecular orientation in the fibers is perhaps due to the existence of the parallel and anti-parallel hydrogen bond interactions between the chain molecules and their supra-molecularly assembled β-pleated sheets. On the other hand, the origin of this anomalous WAXD fiber pattern may be associated with the fact that the fibers were drawn from the S_A^* phase, similar to the example of a series of poly(ester imide)s reported recently [16]. In this report, the drawing process leads to a deformation of smectic blocks rather than stretching of the individual molecules.

The fiber meridian can be assigned as the a^* direction. In the quadrants, there are three layers of reflections that can be observed. For example, the first (1*kl*) layer [instead of (*hk*1) in a normal polymer fiber pattern since the fiber direction is defined as the a^*-direction] possesses six reflections. In the second (2*kl*) layer four reflections are observed. The third (3*kl*) layer has one reflection, etc. Of interest is that the (*h*1*l*) reflections are relatively diffused in Fig. 9 (see arrows in the figure), which are possibly due to the superstructure formation as discussed in previous publications [1,2]. Fig. 10a is an ED pattern for sheared samples, showing the a^*c^* reciprocal plane. As the orientation decreases, the ED spots tend to have an arc-shape (Fig. 10b) and the pattern shows similar features as the WAXD fiber pattern. The (*h*1*l*) arcs in the fiber pattern cannot be observed in Fig. 9b because the sheared ED pattern only presents the a^*c^* reciprocal plane, consisting of (*h*0*l*) diffractions. After careful refinement of the WAXD fiber reflections, the crystal lattice can be determined to be orthorhombic with dimensions of $a = 10.7$, $b = 0.48$ and $c = 5.96$ nm. Table 1 lists the

Table 1
Experimental and calculated crystallographic parameters of the orthorhombic crystal unit cell for annealed PET(R*)-9 fiber at 145°C (the calculated data listed are based on an orthorhombic unit cell with $a = 1.07$, $b = 0.48$, $c = 5.96$ nm, $\alpha = \beta = \gamma 90°$)

(*hkl*)	2θ (°) (cal.)	2θ (°) (exptl.)	*d* (nm) (cal.)	*d* (nm) (exptl.)	Intensity[a]
(002)	2.961	2.971	2.98	2.97	s
(004)	5.925	5.885	1.49	1.50	s
(006)	8.895	8.922	0.993	0.990	s
(008)	11.865	11.930	0.745	0.741	s
(0010)	14.847	14.920	0.596	0. 595	s
(0012)	17.826	17.754	0.497	0.499	m
(102)	8.745	8.833	1.01	1.00	v.s.
(104)	10.167	10.286	0.869	0.859	s
(105)	11.103	11.259	0.796	0.785	m
(108)	14.480	14.552	0.611	0.608	m
(109)	15.722	15.750	0.563	0.562	w
(1010)	16.999	16.901	0.521	0.524	w
(113)	20.778	20.776	0.427	0.428	s
(201)	16.613	16.708	0.533	0.530	v.s.
(205)	18.157	18.309	0.488	0.484	v.s.
(206)	18.819	18.981	0.471	0.467	v.s.
(208)	20.320	20.487	0.434	0.433	m
(305)	26.101	26.337	0.341	0.338	m

[a] The intensities are semi-quantitatively estimated via a microdensitometer. They are classified as very strong (v.s.), strong (s), medium (m), weak (w).

experimental and calculated 2θ and *d*-spacing data for comparison. This result is in excellent agreement with that determined via the SAED technique [1,2].

When crystallization is carried out in the S_A^* phase, both flat-elongated and helical single lamellar crystals can be formed as reported previously, as shown in Fig. 1a [1,2]. Surprisingly enough, the crystal structures of these two crystals are the same. Polyethylene decoration on the surface of the crystals shows that the chain folding direction is along the long axis of the crystals. This reveals that the chain folds towards the less ordered S_A phase rather than along the crystalline planes [1,2]. Therefore, this adds a new factor to the discussion of the crystal growth mechanism of these crystals in the near future. Other findings indicate that not only the lamellar crystal thickness but the length of periodicity as well increase with crystallization temperature [1,2]. Furthermore, the observation in Fig. 1a also suggests that the free energies of forming the flat and helical molecular packing may be comparable, and therefore, both of the morphologies can be observed [2]. Detailed free energy calculations in the crystal structures are required in order to quantitatively analyze this speculation.

Combining the phase transition behaviors with the double-twist chain orientation in the helical lamellar crystals observed recently [3,4], a remarkable similarity of this polymer with biopolymers [5,6,17,18] can be seen, although no hydrogen bonds exist in PET(R*)-9. However, most biopolymers possessing the double-twisted helical packing are in LC states rather than in a three dimensionally ordered crystal, such as in the case of dinoflagellate chromosomes (in *Prorocentrum micans*) which displays the same type of helical structure in an *in vivo* arrangement [17]. *Bombyx mori* silk fibroin can grow a helical lamellar crystal of the β-modification under solution crystallization conditions [18]. Hopefully, the study of the structure, morphology and phase transitions of PET(R*)-9 will initiate a new step in understanding biopolymer behaviors in responses to various environments.

4. Conclusion

In summary, phase structural identifications for a non-racemic chiral PET(R*)-9 have been carried out. This polymer possesses a complicated LC phase behavior. In addition to the normal S_A^* and S_C^* phases, it is the first example for chiral main-chain LC polymers that possesses the TGBA* phase. When crystallization is carried out from the S_A^* phase, both the flat-elongated and double-twisted single helical lamellar crystals can be observed. Based on the WAXD fiber pattern, the structural analysis shows that the crystal unit cell is orthorhombic, which is in agreement with previous ED results. This study may serve as an initiation of establishing relationships among structure, morphology and phase transition behaviors of the non-racemic chiral polymers and finding a pathway to connect phase morphology with biopolymers.

Acknowledgements

This work was supported by the NSF (DMR-9617030) and the NSF ALCOM Science and Technology Center (DMR-8920147). Thoughtful and in-depth discussions with Dr F. Khoury at NIST are gratefully acknowledged. Over the past two years, Professor A. Keller had extensive discussions with us regarding this topic. Many brilliant thoughts from him have and will continue to enlighten and encourage us to further pursue this research.

References

[1] Li CY, Yan D, Cheng SZD, Bai F, He T, Chien LC, Harris FW, Lotz B. Macromolecules 1999;32:524.
[2] Li CY, Yan D, Cheng SZD, Bai F, Ge JJ, He T, Chien LC, Harris FW, Lotz B. Phys Rev B 1999;60:12 675.
[3] Li CY, Cheng SZD, Ge JJ, Bai F, Zhang JZ, Mann IK, Chien LC, Harris FW, Yan D, He T, Lotz B. Phys Rev Lett 1999;83:4558.
[4] Li CY, Cheng SZD, Ge JJ, Bai F, Zhang JZ, Mann IK, Chien LC, Harris FW, Lotz B. J Am Chem Soc 2000;122:72.
[5] Bai F, Chien LC, Li CY, Cheng SZD, Percheck R. Chem Mater 1999;11:1666.
[6] Kleman M. Phys Scr 1987;T19:565.
[7] Kleman M. Rep Prog Phys 1989;52:555.

[8] Ge JJ, Honigfort PS, Ho RM, Wang SY, Harris FW, Cheng SZD. Macromol Chem Phys 1999;200:31.
[9] Pardey R, Harris FW, Cheng SZD, Adduci J, Facinelli JV, Lenz RW. Macromolecules 1992;25:5060.
[10] Pardey R, Shen D, Gabori PA, Harris FW, Cheng SZD, Adduci J, Facinelli JV, Lenz RW. Macromolecules 1993;26:3687.
[11] Yoon Y, Zhang A, Ho RM, Cheng SZD, Percec V, Chu P. Macromolecules 1996;29:294.
[12] Yoon Y, Ho RM, Moon B, Kim D, McCreight KW, Li F, Harris FW, Cheng SZD, Percec V, Chu P. Macromolecules 1996;29:3421.
[13] Goodby JW, Waugh MA, Stein SM, Chin E, Pindak R, Patel JS. Nature 1989;337:449.
[14] Bolton EC, Lacey D, Smith PJ, Goodby JW. Liq Cryst 1992;12:305.
[15] Geddes AJ, Parker KD, Atkins ED, Beighton E. J Mol Biol 1965; 11:706.
[16] Leland M, Zhang A, Ho RM, Cheng SZD, Keller A, Kricheldorf HR. Macromolecules 1997;30:5249.
[17] Livolant F, Bouligand Y. Chromosoma 1980;80:97.
[18] Lotz B, Gonthier-Vassal A, Brack A, Magoshi J. J Mol Biol 1982; 156:345.